JOURNAL OF THERMOPHYSICS AND HEAT TRANSFER
Vol. 20, No. 4, October–December 2006

Modeling of a CO_2–N_2 Plasma Flow in a Supersonic Arcjet Facility

M. Lino da Silva,* F. Passarinho,† and M. Dudeck‡
Centre National de la Recherche Scientifique, 45100 Orléans, France

DOI: 10.2514/1.21641

The Martian-type CO_2–N_2 plasma flow obtained in the plasma generator of the SR5 arcjet facility has been simulated using two complementary fluid descriptions. An inviscid multitemperature monofluid description has firstly been used to evaluate the importance of the different chemical and exchange processes between the flow species. Then, a one-temperature Navier–Stokes description has been used to evaluate the influence of viscous and rarefaction effects. In the nozzle throat region, heat addition from the arc firstly leads to the establishment of a translation-vibration disequilibrium. Near the end of the nozzle throat, temperature and pressure increases allow more efficient exchange processes and lower this disequilibrium. In the nozzle diverging region, chemical and vibrational processes are quickly frozen as the flow strongly expands. Furthermore, a translation-rotation disequilibrium also occurs near the nozzle exit. Navier–Stokes simulation results evidence a quick increase of the diverging section boundary layers, and therefore most of the diverging section is in a fully viscous interaction regime. Moreover, rarefaction effects are predicted to appear near the nozzle exit walls. The experimental measurements carried near the nozzle exit confirm the thermal disequilibrium regime of the flow, predicted by the simulation results.

Nomenclature

anode	=	nozzle anode
arc	=	nozzle electrical arc
cathode	=	nozzle cathode
chamber	=	facility vacuum chamber
Da	=	Damköler number
gas	=	facility gas flow
generator	=	conditions upstream of the nozzle throat
h	=	flow enthalpy, MJ/kg
i	=	chemical species index
Kn	=	Knudsen number
k_B	=	Boltzmann constant, 1.38065×10^{-23} J/K
L	=	characteristic length, m
M	=	flow Mach number
$\dot{m}$	=	mass flow, kg/s
$\dot{Q}$	=	heat transfer rate, kJ/s
p	=	flow pressure, Pa
R–T	=	rotation-translation processes
T	=	flow translational temperature, K
T_{rot}	=	species rotational temperature, K
T_{vib}	=	species vibrational temperature, K
T_w	=	nozzle wall temperature, K
V–D	=	vibration-dissociation processes
V–el	=	vibration-electron processes
V–T	=	vibration-translation processes
V–V	=	vibration-vibration processes
v	=	flow velocity, m/s
$Z(T, T_{\text{vib}})$	=	nonequilibrium coupling factor for dissociation
Z_∞	=	Parker rotational collision number
ΔE	=	energy transfer rate, kW
η	=	arc energy transfer efficiency
ρ	=	flow density, kg/m^3
σ	=	collisional cross-section, m^2
τ_F	=	flow characteristic time, s
τ_{vib}	=	vibrational relaxation characteristic time, s

Received 9 December 2005; revision received 3 March 2006; accepted for publication 3 March 2006.

*Research Scientist, Laboratoire d'Aérothermique, Unit Propre de Recherche 9020. Present address: Centro de Física dos Plasmas, Instituto Superior Técnico, Av. Rovisco Pais, 1049-001 Lisboa, Portugal; mlinodasilva@mail.ist.utl.pt. Member AIAA.

†Graduate Student, Laboratoire d'Aérothermique, Unit Propre de Recherche 9020.

‡Professor, Laboratoire d'Aérothermique, Unit Propre de Recherche 9020. Member AIAA.

I. Introduction

THE simulation of a spacecraft entering a planetary atmosphere in the hypersonic flight regime requires the knowledge of dissociation, ionization and chemical processes, radiative gas phenomena, and nonequilibrium effects on the internal modes. The physical properties of the gas flow surrounding a spacecraft depends on the nature of the molecules present in the planetary atmosphere (Mars and Venus: CO_2–N_2, Titan: N_2–CH_4) but also on the chosen spacecraft trajectory (direct entry, aerobreaking, or aerocapture). Different ground test facilities are available today to simulate such entry conditions (low-pressure hyperenthalpic gas flows): shock tubes, inductive plasma torches, radio-frequency sources, and arcjets [1–4].

Arcjet facilities present the advantage of providing long test runs, performed with stable operating conditions and with appropriate values for several plasma conditions: plasma densities as 10^{11}–10^{13} electrons/cm^3, electron temperatures in the range of 5000–10,000 K, kinetic temperatures around 2000–4000 K, and vibrational temperatures around 8000 K. Some disadvantages include instabilities of the arc source in some operating ranges, cathode erosion effects, and mainly an energy input method somehow different from the phenomena encountered during an atmospheric entry (an electric arc excites the flow electrons, whereas the shock wave produced during an atmospheric entry excites the atomic and molecular species translational mode), yielding different processes for the population of the gas species different internal modes. Nevertheless, arcjet facilities are currently used for the simulation of planetary entry conditions, for carrying heat flux tests on materials for spacecraft protections and for a detailed analysis of the plasma flow [5–8].

Numerical modeling of arcjet plasma sources has to be developed with several goals in mind: determination of the hydrodynamics properties (velocity, pressure, temperature, and Mach number), detailed study of the different physical and relaxation processes (chemical and ionization processes, V–T, V–V, V–D, V–el, and R–T processes), and the development of a numerical tool capable of predicting the behavior of new arcjets.

Several numerical codes have been previously developed to describe the stationary properties of arcjets: Beulens et al. calculated the plasma properties in an arcjet operated with nitrogen, calculating electronic conductivity according to well-known electron-heavy species exchange functions [9]; Kaminska and Dudeck simulated an argon arcjet plasma flow developing a detailed description of dissipative effects using a calculation of transport coefficients by Chapman–Enskog developments and the introduction of anodic and cathodic layers [10]. Flament [11] and William [12] simulated a high-enthalpy stationary flow in a nozzle operating with air, allowing vibrational relaxations for N_2 and O_2 species using a Landau–Teller model. Schönemann et al. [7] investigated a similar problem for a magneto-plasmadynamic (MPD) accelerator using nitrogen or nitrogen-argon mixtures. Navier–Stokes equations have been solved using transport coefficients given by the Yos model and chemical model from Park [13], which includes ionic species. Detailed methods using the state-to-state approximation have also been developed since the 1970s. Such methods are typically restricted to the quasi-1-D approximation for the description of a nozzle expansion, but account for state-resolved processes, including the coupling of free electron kinetics (allowing an accurate modeling of arc discharges) and the influence of metastable states [14–17].

II. Experimental Facility

A. The SR5 Low-Pressure Arcjet Plasma Facility

The SR5 low-pressure arcjet plasma wind tunnel available at the Laboratoire d'Aérothermique has been used during the last years for the simulation of the entry conditions in Earth, Mars, and Titan planetary atmospheres [4]. A dc vortex-stabilized arc operating at low voltages (50–100 V) and low currents (50–150 A) delivers typical powers of 5–10 kW to the flow in the throat region of the nozzle. The low mass-flow rates (0.1–0.5 g/s) crossing the nozzle allows obtaining a high-enthalpy (5–30 MJ/kg) steady plasma jet with a global yield of 50–70%. This level of specific enthalpy obtained with a small mass-flow rate is an advantage because of the low electrode erosion, which allows maintaining a steady plasma jet for several hours with a low level of contamination. The facility pumping system capacity of $26,000\ m^3\ h^{-1}$ ensures an ambient pressure of about 10 Pa to be maintained in a 4.3 m long and 1.1-m-diam vacuum chamber in which the arcjet is expanded.

The arc discharge is generated between the tip of a cathode, which is a small zirconium disk inserted into copper (disk diameter 1.6 mm), and the nozzle throat, which operates as the anode (cylindrical neck of 4 mm length and 4 mm internal diameter, made of tungsten inserted into copper). A zirconium cathode allows reproducing stable plasma flows even with oxygen containing chemical mixtures. Arc discharge is ignited through a high frequency, high voltage pulse (1 MHz, 4000 V). Copper pieces, anode as well as cathode, are water cooled. Balance energy on inlet and outlet water circuit temperatures, measured by thermocouples, is used to determine the efficiency of the plasma generator. The diverging section of the nozzle is 53 mm long with an exit diameter of 48 mm which corresponds to a 25.4 deg half-angle. A schematic view of the nozzle is presented in Fig. 1.

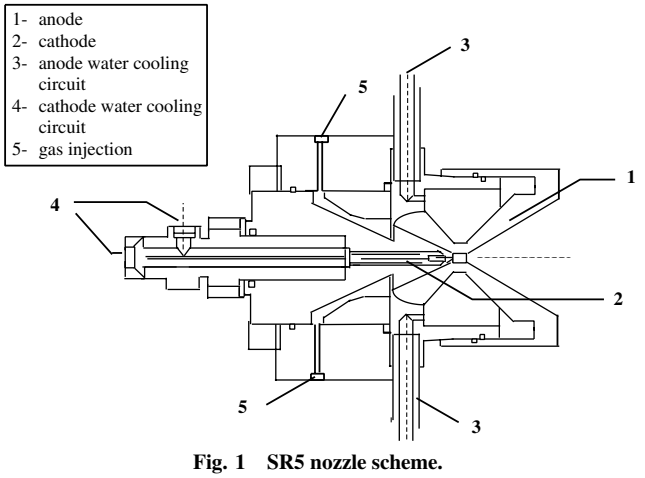

Fig. 1 SR5 nozzle scheme.

B. Simulation of Martian-Type Plasmas in the SR5 Facility

An experimental research program investigating Martian atmospheric entry plasmas radiation has been conducted over the last years in the low-pressure arcjet facility SR5, available at the Laboratoire d'Aérothermique [18]. In the scope of this program, CO_2–N_2 Martian plasma flows have been simulated in the SR5 facility. Here, the experiment parameters were set to reproduce closely the conditions encountered during the critical phase of a Martian atmospheric entry. In the course of this research program, extensive emission spectroscopy measurements were carried out near the facility nozzle exit, providing experimental results for some emitting species characteristic rotational and vibrational temperatures. Optical emission spectroscopy diagnostics are the only available tool for investigating the arcjet plasma generator flow properties; no measurements can be carried out inside the arcjet plasma source, and the measurements in the nozzle exit plane cannot be carried out using intrusive diagnostics due to the high level of energy transfer found in this region. Therefore, to improve the description of this facility arcjet (a convergent-divergent nozzle with an electrical arc discharge in the nozzle throat), it has been decided to develop several numerical models for describing such a nozzle flow.

The numerical models used in this study are presented in Sec. III. The simulation results are presented in Sec. IV, and finally some comparisons with experimental results are presented in Sec. V.

III. Numerical Models

Supersonic arcjet wind tunnels are typically one of the most challenging facilities for numerical modeling. The upstream conditions in the arcjet generator are not well known, as the discharge region usually cannot be accessed through any intrusive or optical diagnostics. Also, modeling of the plasma arc is a very challenging task, as exact numerical models require a two-fluid (electrons and heavy species) numerical description. As mentioned before, such descriptions have only been successfully applied to the description of simpler argon and nitrogen flows [9,10], and many issues regarding the physical and numerical models used in such numerical descriptions remain to be solved. Therefore, such fluid descriptions still cannot be systematically applied for the description of general arcjet plasma flows. For example, CO_2–N_2 flows require the use of complex chemical models for the description of electron-impact dissociation and ionization processes, which prevents setting up a physically accurate description of the electrical arc energy input in the plasma generator. Instead, a classical monofluid approach has been kept, using a simplified description of the electrical arc energy input.

The numerical code ARES, developed by the CEA-CESTAS, has been used to describe the plasma flow inside the generator. The code solves the bidimensional Navier–Stokes equations for high-enthalpy flows, using a one-temperature description. However, the code has not the ability of simulating energy addition phenomena, thus preventing the authors from simulating the nozzle throat flowfield, where energy addition from the electric arc occurs.

In parallel, it has been chosen to develop a simpler one-dimensional numerical code. Care was exercised in developing a more detailed thermodynamic database, allowing the application of a multitemperature model (accounting for the flow translational temperature and the species-dependent rotational and vibrational temperatures). This approach allows us to carry a detailed analysis of the thermodynamic relaxation processes encountered in the flow, without large calculation time requirements. Energy addition processes have also been considered in this numerical code, but some restrictions and assumptions have to be considered if the flow in the nozzle throat is to be modeled using a quasi-1-D description:

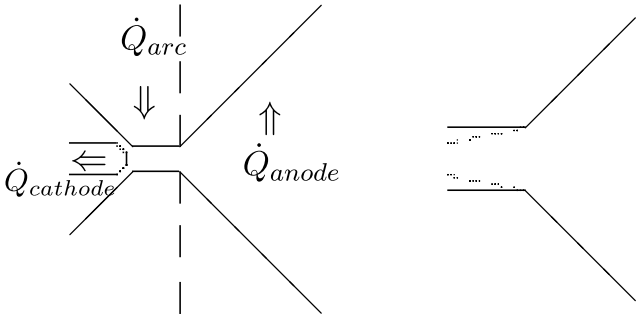

Fig. 2 Nozzle simulation model.

1) The flow is assumed to enter the throat of the nozzle at sonic conditions, as the nozzle anode laminates the gas flow. The upstream conditions (such as mass flow, pressure, speed and area cross-section) being known, it is possible to determine flow parameters at the throat entry making use of the Euler relations, if the flow is treated as an ideal gas and pressure losses are neglected in the inlet gas tube.

2) The throat entry cross-section being smaller than the exit cross-section, due to the choking effects of the cathode, the throat can be modeled as a diverging section (see Fig. 2, right side). Energy is added to the fluid through an arc discharge between the cathode and a tungsten insert in the nozzle throat which acts as an anode. This is modeled as a constant energy deposition through the 4 mm section of the throat.

3) The tungsten tip being heat refractive, water cooling of the nozzle is assumed to remove energy from the flow uniquely in its geometrically diverging section. Moreover, in the diverging section, the center streamline is assumed not to be influenced by energy removal effects at the wall boundary.

This simplified model of the nozzle is schematically depicted in Fig. 2.

In short, the 1-D thermal nonequilibrium code has been applied to the simulation of the nozzle throat flow, applying the aforementioned simplifying assumptions regarding the heat addition to the flow from the electrical arc.

Some of the aforementioned assumptions are somehow restrictive as here we consider the electrical arc to heat the species translational modes, which then redistribute such energy to the other internal modes (rotational, vibrational, chemistry). Instead, the electrical arc is known to transfer its energy to the flow free-electrons, which then redistribute this energy to the flow heavy species through electron-impact reactions.

The assumption of a constant heat addition had, however, to be retained, as our numerical code is currently unable to solve the Boltzmann equation in presence of an electrical field. Moreover, electron-impact processes, or the influence of metastable states in CO_2–N_2 flows are not yet well known. Furthermore, it will be verified more ahead that the energy transfer by the electrical arc strongly increases the temperature and pressure of the nozzle throat flow. The energy between the different species internal modes is therefore efficiently redistributed, leading the flow to a state close to thermal equilibrium near the nozzle throat exit. This way the modeling of the energy transfer process in the nozzle throat region has a limited impact on the flow properties in the diverging section.

Departing from the determined flow properties in the nozzle throat exit, the flow expansion in the nozzle diverging section has then been simulated using both the 1-D thermal nonequilibrium, and the 2-D Navier–Stokes codes. This has allowed the examination of, respectively, the influence of thermal nonequilibrium and dissipative and rarefaction effects on the flow macroscopic properties.

A. Detailed Description of the 1-D Thermal Nonequilibrium Code

The simplified numerical code which has been developed solves the Euler flow equations using the quasi-1-D approximation. The code includes a thermodynamic database which allows taking into account the different chemical reactions and energy exchange processes between the flow's chemical species. The thermochemical model assumes a Boltzmann equilibrium of the species rotational and vibrational modes (unlike more precise but also more complex state-to-state models). A more complete description of this code can be found in [18].

Rotational and vibrational modes relaxation for each molecule are solved in the usual way using the Landau–Teller relation [19]. The rotational collision parameter used in the equation proposed by Parker [19] for the calculation of *R–T* processes is given in this last reference for N_2 and O_2. In absence of further data, such a parameter has been arbitrarily set equal to the value of N_2 for the other molecules. *R–T* processes can then be calculated in the usual way. The rate coefficients for vibrational-translational and vibrational-vibrational processes are issued from the expressions of Millikan and White [20] updated by Park [13] for air-type species collisions, and from Losev et al. [21] for Martian-type species collisions. Vibration-dissociation processes are taken into account by adding a nonequilibrium factor. This factor is calculated according to the relation proposed by Shatalov and Losev [22], without accounting for vibrational energy losses/gains through dissociation/recombination. Finally, a total of 108 *V–T*, 44 *V–V*, and 100 *R–T* processes are included in the code database to allow thermal nonequilibrium calculations for CO_2–N_2 and N_2–O_2 flows.

B. Detailed Description of the 2-D Navier–Stokes Code

The ARES code is a 2-D structured, chemically reacting Navier–Stokes code. It uses a Harten–Yee method, with a Riemann solver over a Roe's matrix verifying the properties of a locally out of thermodynamic equilibrium (LOTE) gas. The code can be executed in explicit or implicit mode, first or second order. A space marching or time marching technique can be used. The flow can be treated as a perfect gas, a real gas, a chemical nonequilibrium gas ($Da \simeq 1$), or a frozen gas ($Da \gg 1$). Also, the flow can be considered to be in the laminar, transitional, or turbulent regime. Viscosity coefficients can be calculated according to Pant, Sutherland, Gibbs, and Wilke [23] laws when applicable. Thermal conductivity can be calculated using tabulated values, assuming a constant Prandtl number or using Wilke law [23]. Diffusive fluxes can be evaluated using Fick's law and assuming a constant Lewis number, or using the more general Chapman–Enskog law [24]. Viscosity coefficients using the Blottner [25] law as well as thermodynamic parameters of the different species for CO_2–N_2 and N_2–O_2 flows are issued from William [12].

IV. Simulation Results

To be able to compare the hydrodynamic simulations results with available experimental data, the numerical codes were applied to the reproduction of a specific plasma flow obtained in the SR5 facility, where experimental data was measured. The flow parameters are listed in Table 1. [§]

As the quasi-1-D code uses a simplified flow model and neglects dissipative effects, the obtained results were investigated quantitatively, with an analysis of the relative importance of the different exchange processes between the flow different chemical species. This analysis was completed with an investigation of the importance of the dissipative effects in the nozzle diverging section, using the ARES code. These two issues will be discussed in Secs. IV.A and IV.B

A. Assessment of the Different Physical-Chemical Exchanges in the Plasma Generator

A 1-D calculation taking into account all the exchange processes included in the code was firstly carried out to evaluate the different departures from thermochemical equilibrium present in the nozzle flow. A simulation has been carried out taking into account chemical, *V–T*, *V–V*, *V–D*, and *R–T* processes, and including the three vibrational modes of the CO_2 molecule. Translational temperature, molecular vibrational temperature, and rotational temperature have

[§]One standard litre per minute corresponds to 22.4 mol per minute at 298 K

Table 1 CO_2–N_2 plasma parameters

Experience Parameters			
$\dot{m}_{CO_2}$	14.72 slm	ΔE_{arc}	+7.44 kW
$\dot{m}_{N_2}$	0.45 slm	$\Delta E_{cathode}$	−0.64 kW
$\dot{m}$	0.45 g/s	$\Delta E_{cathode}$	−3.00 kW
$p_{generator}$	49,600 Pa	h_{gas}	8.4 MJ/kg
$p_{chamber}$	4.9 Pa	η	51%

been calculated in the nozzle throat and diverging section and are plotted in Fig. 3.

Vibrational nonequilibrium is present in the nozzle throat, as for low temperatures, the characteristic vibration times for the different molecules present in the flow are lower than the flow residence time [$\tau_{vib_i} \in (10^{-4}\text{ s}–10\text{ s}) < \tau_F \sim 10^{-7}$ s]. Dissociation effects become apparent after about 2.5 mm from the nozzle throat. The vibrational temperatures of N_2, CO, $CO_2(\nu_2)$, and $CO_2(\nu_3)$ follow the same trends as O_2 and $CO_2(\nu_1)$, but with a more marked behavior. For the C_2 and CN molecules, vibrational temperatures remain lower near the nozzle throat inlet, lately rising to values comprised between the two aforementioned groups of vibrational temperatures. The behavior of the NO vibrational temperature is close to the behavior of O_2 and $CO_2(\nu_1)$ vibrational temperatures. As the flow reaches higher temperatures, the different vibrational characteristic times become lower ($\tau_{vib_i} \sim 10^{-5}$ s), without, however, allowing vibrational equilibration with the flow translational temperature to occur. In the diverging section, rarefaction effects increase the thermal nonequilibrium between T and $(T_{vib})_i$, with more or less quick freezing of the latter temperatures.

As expected in regard of the sufficiently high densities in the nozzle throat, a rotational-translational equilibrium is achieved in the nozzle throat. Rarefaction effects in the diverging section lead to a thermal nonequilibrium between translational and rotational temperatures (around 1000 K after about 10 mm from the nozzle throat exit), without, however, a freezing of the latter. The different rotational temperatures remain nearly equivalent, as their R–T collisional parameters are similar.

Chemical composition of the flow in the nozzle throat and diverging section, as well as the effects of molecular vibration over the chemical reactions, are presented in Fig. 4. The main apparent effect is the dissociation of the CO_2 molecule as soon as the translational temperature becomes sufficiently high. The concentration of molecular nitrogen is quite constant and the molecular oxygen concentration is negligible, only reaching a few percent of atomic oxygen at the throat exit. Moreover, the concentrations inside the throat are not in chemical equilibrium conditions regarding the local kinetic temperature and pressure.

It is verified that adding V–D coupling effects to chemistry calculations has the effect of slowing dissociation reactions in the nozzle flow (mainly dissociation of CO_2 into CO and O) as the different vibrational temperatures are smaller than T. Also, the

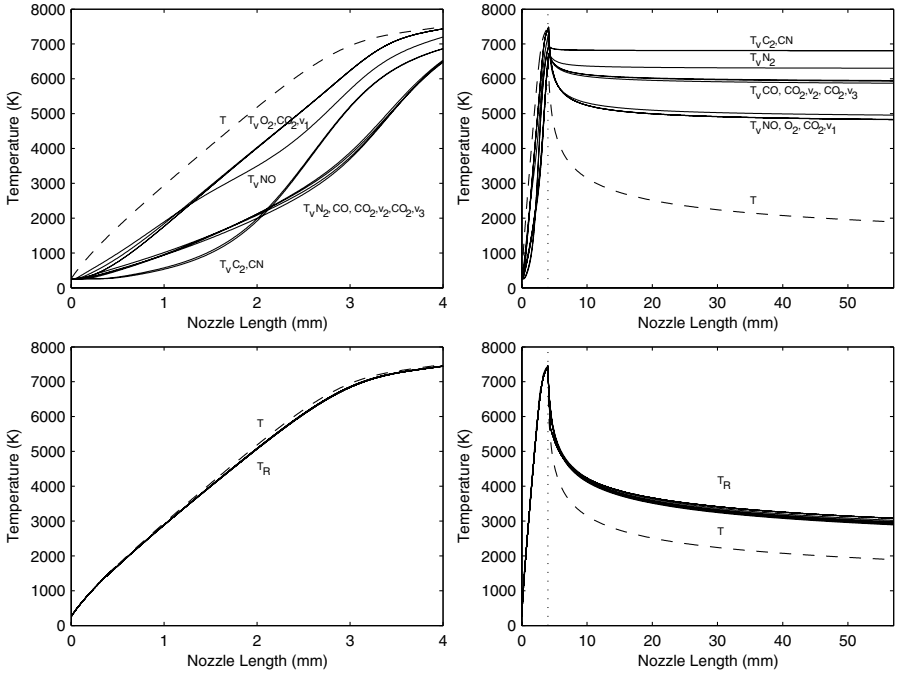

Fig. 3 Vibrational (top) and rotational (bottom) temperatures of the molecular species in the nozzle throat (left) and diverging section (right).

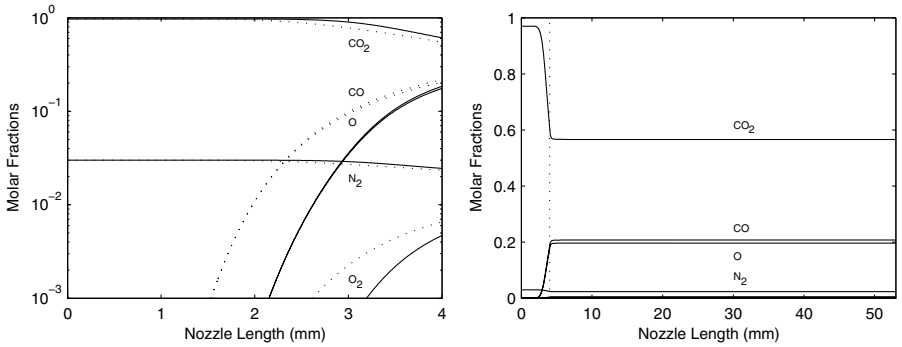

Fig. 4 Molar fractions in the nozzle throat (left) with (solid lines) and without (dotted lines) V–D coupling; in the nozzle throat and diverging section with V–D coupling (right).

Table 2 Plasma translational temperatures (K) with different processes considered

	Nozzle throat exit	Nozzle exit
Chemical, *V–T*, *V–V*, *V–D*, *R–T*	7496	1893
Chemical, *V–T*, *V–V*, *V–D*	7494	2096
Chemical, *V–T*, *V–V*	7144	1921
Chemical,*V–T*	7142	1927
Chemical	7153	2107
Frozen	9019	4052

sudden expansion of the flow in the diverging section freezes the chemical composition of the flow almost instantaneously, preventing any recombination reactions from happening in the nozzle diverging section. This expansion is characterized by a pressure decreasing from about 30,000 to 30 Pa in the nozzle exit.

This study has been completed by an analysis of the different nonequilibrium processes on the flow macroscopic parameters (translational temperature, pressure, and Mach number). Knowledge of the influence of such nonequilibrium processes over these macroscopic parameters allows determining the suitability of carrying loosely coupled calculations using a more accurate description of the flow macroscopic parameters and including accurate nonequilibrium models. This would allow overcoming the flaws of the presently used models, as accurate fluid descriptions such as 2-D or 3-D Navier–Stokes calculations usually account solely for a restricted set of nonequilibrium processes [18]. On the other hand, accurate models of nonequilibrium processes (such as state-to-state models) are often included with simplified fluid mechanics descriptions; typically 1-D [14,26], and fully coupled calculations still remain computationally intensive [27]. Loosely coupled calculations present several advantages over fully coupled calculations: calculation times can be largely reduced with such a scheme, numerical convergence issues are less likely to appear, and one may choose whose thermodynamical and gas kinetics models are to be included in a specific calculation. For several applications, in which nonequilibrium effects are limited, this may be a promising approach.

Here, calculations have been carried using the same input conditions of the flow (see Table 1), but the different nonequilibrium processes in the flow were successfully disregarded. The obtained translational temperature values obtained at the end of the nozzle throat and at the nozzle exit are presented in Table 2.

Values for the different flow macroscopic parameters T, p, and M in the overall nozzle with and without an accounting for these different interactions are plotted in Fig. 5.

We conclude that the translational temperature in the nozzle throat flow is only sensibly affected by the chemistry. *V–D* processes will hinder the flow chemistry composed of endothermical reactions, therefore allowing higher flow translational temperatures. On the contrary, *V–T*, *V–V*, and *R–T* processes are negligible in this region of the flow. In the nozzle diverging section, *V–T* and *R–T* processes alter the translational temperature for about 200 K. The temperature differences due to *V–D* processes and chemistry are merely a consequence of the already higher temperature in the nozzle throat exit as the flow is frozen in the diverging section. Finally, it can be verified that only chemical processes affect sensibly the flow translational temperature. The other processes can be neglected if one solely wants to determine this quantity. Similar trends can be expected for the other flow macroscopic parameters p and T as all these are linked through the flow macroscopic parameters.

The small effect of vibrational and rotational nonequilibrium on the flow macroscopic parameters, and the moderate effect on the flow chemical composition (*V–D* processes) allows considering carrying out one-temperature Navier–Stokes calculations using the ARES code to obtain reliable results for the flow macroscopic parameters.

B. Assessment of the Dissipative Effects in the Plasma Generator Diverging Section

Carrying out a Navier–Stokes simulation in the nozzle diverging section firstly requires a knowledge of the boundary conditions of the problem. The inlet conditions are provided by the nozzle throat quasi-1-D simulation results. However, it is furthermore necessary to know the wall boundary parameters in the diverging section, and these are typically unknown (although the heat loss rates are known, the nozzle geometry is a complex one to model thermically, and the boundaries contact factors are unknown). Here it has been arbitrarily chosen to enforce a wall temperature $T_w = 800$ K.

Flowfield simulations using the ARES code have been carried out using a 65×40 grid refined near the throat and along the wall. Use of the nozzle axisymmetry was made when creating the grid (see Fig. 6). The grid size and aperture has been selected such that halving the grid size will lead to different calculated flowfields, and doubling it will lead to identical flowfields. This way, grid convergence has been enforced. A grid size of 0.2 μm is obtained near the wall.

As it has been verified using the quasi-1-D thermal nonequilibrium description, exchange processes and chemical reactions between the different species of the flow are frozen throughout the overall nozzle diverging section, and have been considered as so (frozen flow) in the ARES Navier–Stokes simulation. Moreover, the flow has been assumed as laminar (a reasonable assumption in view of the low

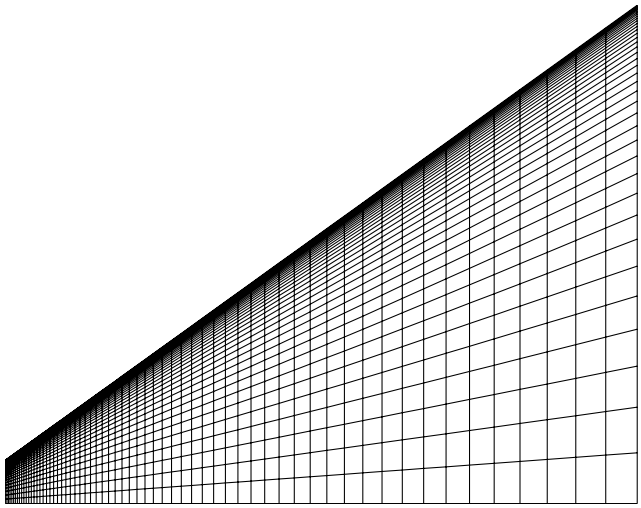

Fig. 6 Nozzle computational grid.

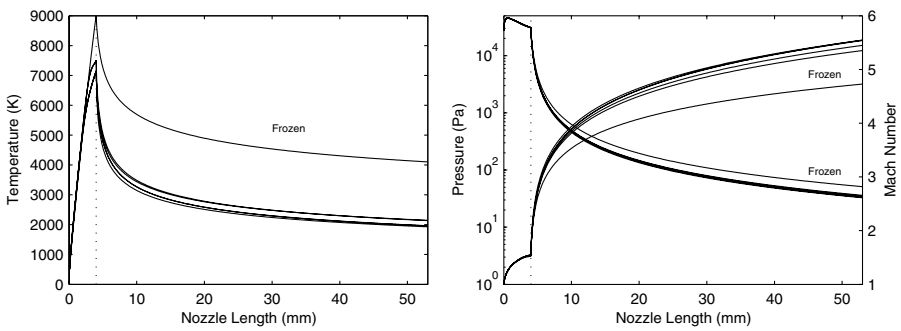

Fig. 5 Temperature plots (left), pressure and Mach number plots (right), accounting for the different processes (see Table 2).

pressure of the flow) and a constant Lewis number of 1 has been used for the calculation of diffusive fluxes. A run of the ARES code has also been carried using an Euler inviscid description, so as to evaluate the influence of dissipative effects on the flow macroscopic parameters, but also to evaluate the differences of a quasi-1-D and 1-D axisymmetric Euler description of the SR5 nozzle flow.

A first comparison of the obtained results can be shown for the Mach number profiles of the diverging section center streamline (see Fig. 7), using the same inlet and boundary conditions.

Two conclusions can be drawn. Firstly, as it can be expected, the quasi-1-D approach is inadequate for describing the diverging section flowfield, owing to the nozzle high divergence angle. Moreover, besides the quick rarefaction of the flow, viscous effects are dominant throughout the overall nozzle diverging section. As early as 5 mm from the nozzle throat exit, the center streamline velocities start diverging, achieving a terminal velocity of $M = 4.9$ for the Navier–Stokes description and $M = 6$ for the Euler description.

Therefore, it is concluded that only the Navier–Stokes description can adequately describe the flow macroscopic parameters (velocity, temperature, pressure) in the nozzle diverging section. The fact that the ARES code only accounts for a one-temperature flow description does not preclude it from yielding accurate results regarding the flow macroscopic properties. Indeed, it has been verified in Sec. IV.A that the exchange processes between the species internal modes have a limited effect on the flow macroscopic properties.

The obtained Mach number and translational temperature profiles are presented in Figs. 8 and 9.

Once more, the predominance of the viscous effects throughout the overall nozzle can be verified from the examination of the Navier–Stokes simulation results. The plasma flow appears in supersonic conditions throughout most of the nozzle exit section, the sonic line being located near the nozzle walls, in the flow boundary layer. Furthermore the nozzle wall-cooling effects, accounted for in the Navier–Stokes simulation, lead to a lower translational temperature in the nozzle exit (1577 K for the center streamline). This temperature is lower than the ones obtained using with the quasi-1-D description, which does not account for the nozzle-cooling effects.

C. Assessment of the Flow Rarefaction Effects in the Diverging Section

To check on the flow rarefaction degree in the nozzle diverging section, the Knudsen number has then been calculated according to the relationship [28]

$$Kn = \frac{Tk_B}{[p + \rho(v^2/2)]\sqrt{2}\sigma L} \tag{1}$$

Here, the characteristic length L is the local nozzle diameter, and the collisional cross-section has been taken as $\sigma = 10^{-19}$ m^2 [29].

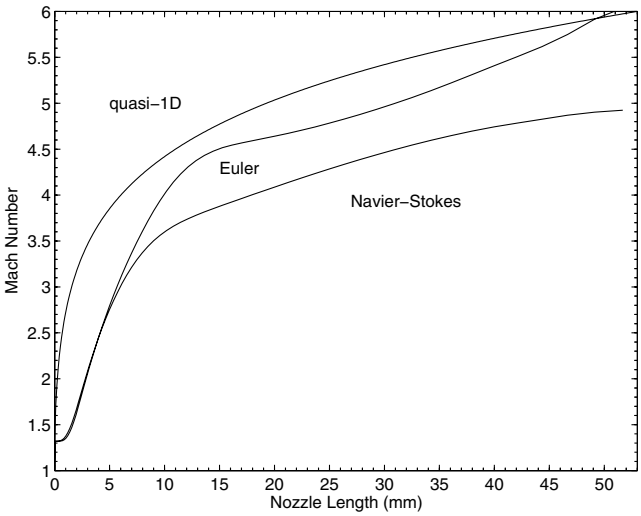

Fig. 7 Calculated Mach number profiles in the center streamline.

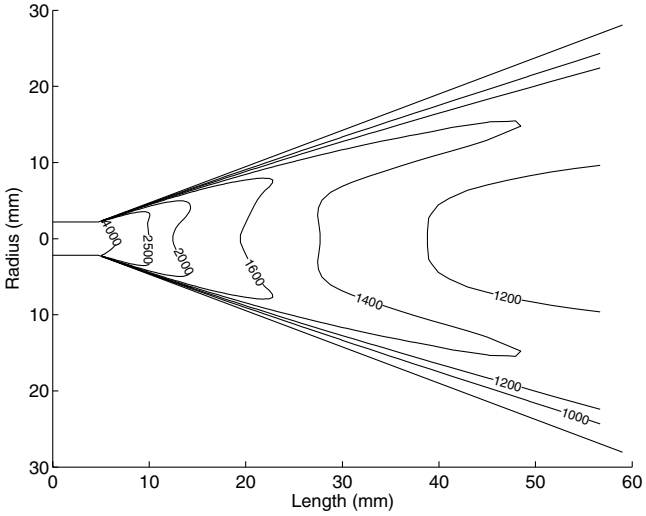

Fig. 9 Calculated temperature profiles in the nozzle diverging section.

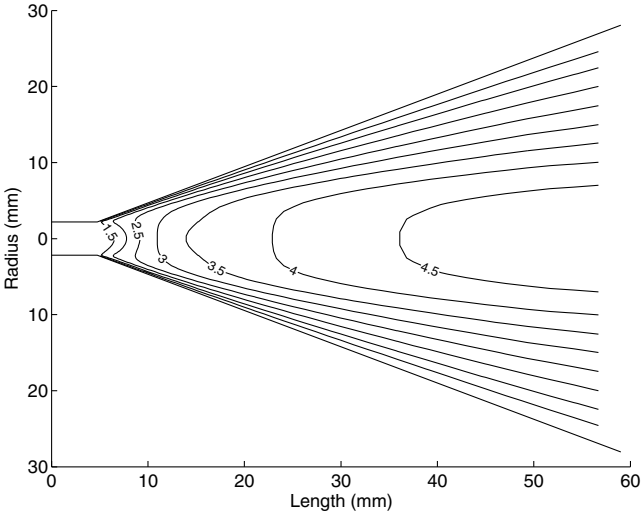

Fig. 8 Calculated Mach number profiles in the nozzle diverging section.

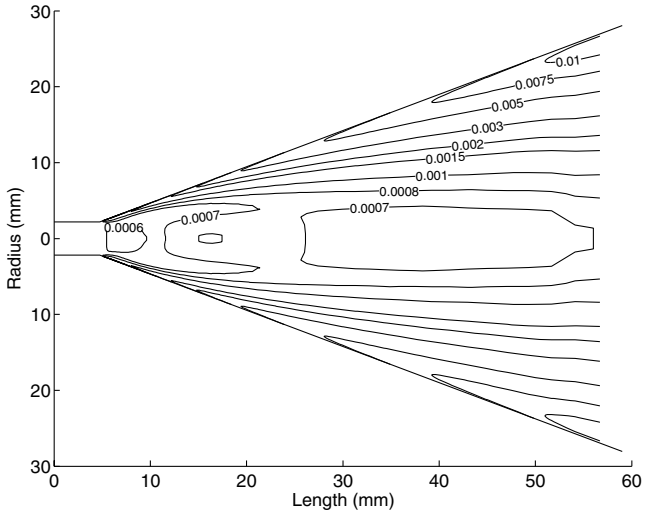

Fig. 10 Calculated Knudsen number profiles in the nozzle diverging section.

The Knudsen number profiles inside the nozzle diverging section are presented in Fig. 10

It is verified that near the nozzle wall region, at about 50% of the nozzle length, the Knudsen number reaches values as high as $5–10 \times 10^{-3}$ and may be considered close to the slip regime ($Kn \geq 10^{-2}$). Therefore, in future studies, it may be necessary to enforce a slip condition near the wall, allowing nonzero velocities of the flow. This has not been considered in this work, as the ARES code does not allow considering gradual transitions to the slip regime. Another important conclusion, regarding the nozzle exit pressure range of 100–170 Pa and the vacuum chamber pressure of 5 Pa, is that the expansion of the plasma plume inside the vacuum chamber will lead the flow to the transitional or even free-molecular regime.

V. Experimental Validation

The obtained simulation results already allow drawing some general considerations regarding the physical properties of the SR5 facility simulated CO_2–N_2 flows.

The main conclusions are 1) the strong expansion of the flow leads the species vibrational and rotational modes to quickly freeze, leading to a strong thermal nonequilibrium near the nozzle exit; and 2) viscous effects are dominant throughout the overall nozzle diverging section. However, the predictive capabilities of the numerical codes can only be assessed by comparing numerical data against experimentally determined data.

A. Qualitative Assessment of the Flow Supersonic Condition

In many small-scale plasma facilities, the assessment of whether the flow has indeed achieved the rarefied supersonic flight regime near the nozzle exit is a difficult task. Phenomena like heat blockage of the nozzle flow, the presence of a normal shock inside the nozzle, or even the inability to achieve sonic conditions in the nozzle throat, may prevent obtaining supersonic flows in the nozzle exit for given experimental conditions (mass flow, arc power, etc.). Therefore, the starting point of any experimental validation should be the determination of the flow regime (supersonic/subsonic) at the nozzle exit.

To determine the flow velocity in the plasma plume, several diagnostics can be used. Laser-induced fluorescence (LIF) diagnostics have been used for an argon-nitrogen plasma flow [30], and crossed electrostatic probes have been used for argon and air plasmas [31], but not near the nozzle exit where such diagnostics are unable to withstand the high temperatures encountered in such the region of the flow. Here, electrostatic probes measurements have been carried using the time-of-flight method. Two single electrostatic probes were aligned at a defined distance with the plasma flow near the nozzle exit, and a "sawtooth" electric signal was applied to the plasma arc using a voltage modulator. However, conclusive results could not be reached, and the technique is still under improvement.

Instead, a simpler method was used. A metallic sphere was inserted in the flow, and an intensified camera was used for measuring the overall plasma radiative emission in the visible range. Should the plasma flow be in the supersonic regime, a bow-shock would be created in front of the metallic sphere, which could be detected as an increase of the radiative emission in this region (due to the density increase, and the possible excitation of the flow radiative states through the shock). Indeed, the presence of a bow-shock in front of the sphere has been detected as it can be verified in Fig. 11. The supersonic regime of the plasma flow has therefore been asserted using this simplified technique.

B. Measurement of the Species Characteristic Temperatures, and Comparison with Calculated Values

One effective technique for validating some of the obtained results is optical emission spectroscopy. Provided that molecular radiative systems are measured near the nozzle exit, the molecule vibrational and rotational temperatures can be determined. In the SR5 facility, a high resolution spectrometer is available for probing the plasma radiative emission in the 300–950 nm range. For Martian-type CO_2–N_2 flows, the emission of the CN violet system and of the C_2 swan bands is observed [18]. However, the excited state $d^3\Pi$ of the C_2 swan bands is populated by recombination processes of atomic carbon [32–34], leading to population inversions and strong nonequilibrium effects regarding the molecular transition excited and ground states. Finally, only the CN violet system is suited for an experimental validation of the calculated internal modes populations. Spectral measurements of this radiative system have been carried out throughout the overall nozzle exit section, and finally, because of the axisymmetry of the plasma flow, the Abel-inversion technique has been applied to obtain the local emissive spectra in the nozzle exit center. This measured spectrum has then been reproduced using a line-by-line spectral code [35]. Previous investigations have evidenced the absence of a Boltzmann equilibrium in the population of the CN vibrational levels, likely due to an optical pumping phenomena [18]. However, the rotational levels have been found to follow a Boltzmann distribution, and therefore not only the CN rotational temperature but also the relative populations of the CN vibrational levels have been iterated until a best fit has been achieved. The fitting procedure has been carried as follows: A first estimate of the normalized vibrational levels populations has been assumed, along with an estimated rotational temperature. Then, through visual comparison of the simulated and experimental spectra, the vibrational levels populations have been adjusted until an optimized fit has been achieved. Finally, holding the same vibrational levels populations, the rotational temperature has been iterated until a best fit has

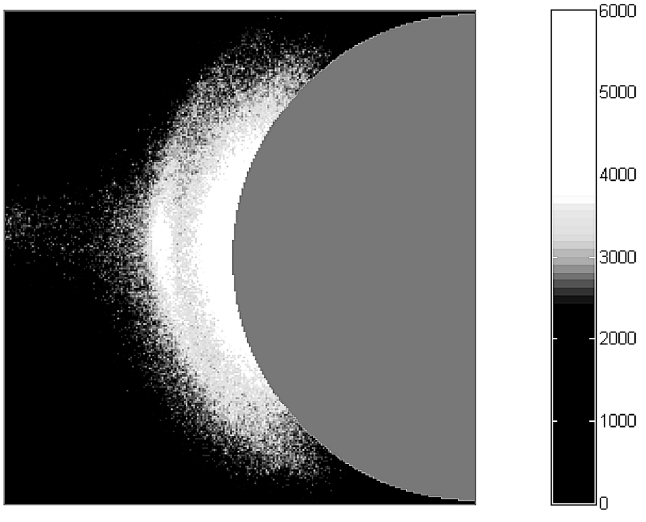

Fig. 11 Radiative intensity near the metallic sphere (arbitrary units).

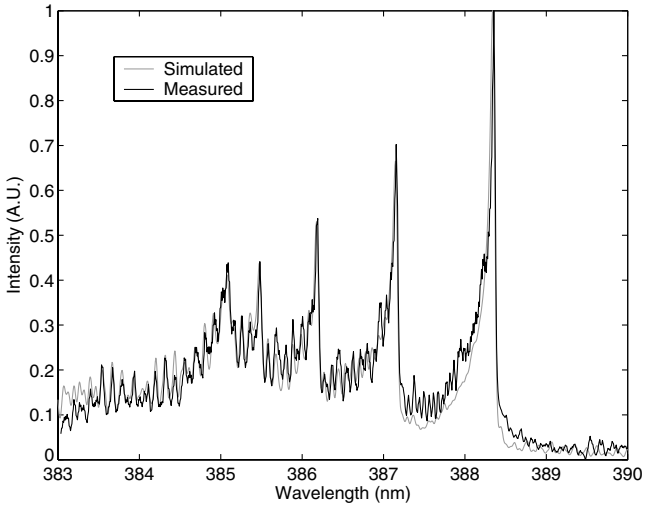

Fig. 12 Comparison between the measured and simulated CN violet ($\Delta v = 0$) spectra.

been achieved. The uncertainties for this rotational temperature have finally been determined as follows: The best fit temperature has been slowly varied until a visual comparison of the two spectra showed that the fit was no longer adequate. The comparison between the experimentally determined spectra and the best fit of the reproduced spectra is presented in Fig. 12.

For the numerical fit, optimized against the measured spectrum, the rotational temperature of the CN molecule has been found to be $T_{\text{rot}} = 2700 \pm 200$ K. This value is to be compared with the different numerically obtained temperature quantities. The ARES code yields a translational temperature of about 1600 K, and the quasi-1-D code yields a rotational temperature of about 3050 K for the CN molecule. From the comparison of these numerical and simulated values it can be easily seen that the measured rotational temperature is very close to the calculated rotational temperature for the CN molecule. Moreover, these two temperatures are very different from the flow calculated translational temperature, which is about 1000–1500 K lower. This allows concluding that indeed the rotational and translational modes of the flow molecular species are very likely to be in disequilibrium. Future experimental determinations of the flow translational temperature would likely detect a much lower flow translational temperature in this region of the flow.

VI. Conclusions

This work has mainly allowed reaching a more detailed qualitative understanding of the physical-chemical phenomena encountered in the SR5 plasma generator. The difficult issues of simulation of such complex flows as arcjet plasma flows have been coped with by using different but complementary flow descriptions. The application of a simplified quasi-1-D flow description with a detailed thermochemical nonequilibrium model has brought to evidence that 1) species concentrations and vibrational temperatures are quickly frozen in the nozzle diverging section, due to the very strong expansion experienced by the flow; 2) the flow species rotational temperatures have slower relaxation times that the flow translational temperature, leading to a translational-rotational nonequilibrium near the nozzle exit; and 3) exchange processes other than chemical reactions have a limited influence on the flow macroscopic properties.

These firstly established conclusions have allowed us to carry more detailed Navier–Stokes calculations on the nozzle diverging section, but using a one-temperature description, and considering a chemically frozen flow. Moreover, the flow inlet parameters were obtained from the quasi-1-D code results, taking into account the approximations described in Sec. III. The Navier–Stokes calculation results have shown that viscous and dissipative effects are dominant in the nozzle diverging section, precluding the use of more simplified Euler descriptions of the flow. Moreover, rarefaction effects are predicted to become important near the nozzle exit.

Some conclusions can be drawn from the examination of the numerical results obtained in this work. It is possible to consider carrying loosely-coupled calculations using a precise Navier–Stokes description of the flow macroscopic parameters, alongside a detailed description of the reactions and interactions between the flow species internal modes. Other preliminary results have already been obtained for a calculation using a loosely-coupled Navier–Stokes and state-to-state description for N_2–O_2 flows [36], and will be extended to the description of CO_2–N_2 flows [37].

The experimental validations carried so far, using emission spectroscopy techniques, have allowed us to unambiguously determine the supersonic regime of the flow near the nozzle exit, and have confirmed the existence of a thermal disequilibrium of the flow species translational and rotational temperatures. Further validations, using LIF techniques, have been so far unsuccessful. Difficulties concerning low signal return from the probed radiative transitions of atomic oxygen[‖] have precluded the achievement of experimental measurements of flow properties such as velocity and translational temperatures. These issues require more extensive experimental validation campaigns.

[‖]Private communication from E. Pawelec and S. Mazouffre, 2004

Acknowledgments

The authors would like to acknowledge E. Pawelec and S. Mazouffre for fruitful discussions on LIF diagnostics in the SR5 facility. The authors would also like to acknowledge the reviewers of this article for helping to improve the manuscript.

References

[1] Boubert, P., Chaix, A., Chikhaoui, A., Robin, L., and Vervisch, P., "Aerodynamic Calibration of TCM2 Facility and Study of a Bow Shock Layer by Emission and Laser Spectroscopy," *Shock Waves*, Vol. 11, No. 5, 2002, pp. 341–351.

[2] Laux, C. O., Spence, T. G., Kruger, C. H., and Zare, R. N., "Optical Diagnostics of Atmospheric Pressure Air Plasmas," *Plasma Sources Science and Technology*, Vol. 12, No. 2, 2003, pp. 125–138.

[3] De Benedictis, S., Cramarossa, F., and d'Agostino, R., "Infrared and Visible Analysis of $He-CO$ and $He-CO-O_2$ Radiofrequency Discharges," *Journal of Physics D: Applied Physics*, Vol. 18, No. 3, 1985, pp. 413–423.

[4] Lago, V., Lebéhot, A., Dudeck, M., Pellerin, S., Renault, T. and Echegut, P., "Entry Conditions in Planetary Atmospheres: Emission Spectroscopy of Molecular Plasma Arcjets," *Journal of Thermophysics and Heat Transfer*, Vol. 15, No. 2, 2001, pp. 168–175.

[5] Scott, C. D., "Survey of Measurements of Flow Properties in Arcjets," *Journal of Thermophysics and Heat Transfer*, Vol. 7, No. 1, 1993, pp. 9–24.

[6] Boubert, P., and Vervish, P., "CN Spectroscopy and Physico-Chemistry in the Boundary Layer of a C/SiC Tile in a Low Pressure Nitrogen/Carbon Dioxide Plasma Flow," *Journal of Chemical Physics*, Vol. 112, No. 23, 2000, pp. 10482–10490.

[7] Schönemann, A. T., Auweter–Kurtz, M., Habiger, H. A., Sleziona, P. C., and Stöckle, T., "Experimental and Numerical Investigation of the Influence of Argon Used as Protection Gas in a Reentry Simulation Device," AIAA Paper 93-2829, July 1993.

[8] Schönemann, A. T., Lago, V., and Dudeck, M., "Mass Spectrometry and Optical Spectroscopy in N_2-CO_2 and N_2-CH_4 Plasma Jets," *Journal of Thermophysics and Heat Transfer*, Vol. 10, No. 3, 1996, pp. 419–425.

[9] Beulens, J. J., Milojevic, D., Schram, D. C., and Vallinga, P. M., "A Two-Dimensional Nonequilibrium Model of Cascaded Arc Plasma Flows," *Physics of Fluids B: Plasma Physics*, Vol. 3, No. 9, 1991, pp. 2548–2557.

[10] Kaminska, A., and Dudeck, M., "Modelling of Non-Equilibrium Arc-Jet Plasma Flow," *Journal of Technical Physics*, Vol. 40, No. 2, 1999, pp. 33–40.

[11] Flament, C., "Écoulements de Fluides Visqueux en Déséquiibre Chimique et Vibrationel. Modélisation. Applications Internes et Externes," Ph.D. Thesis (in French), Université Paris VI, Paris, Nov. 1990.

[12] William, J., "Étude des Processus Physico–Chimiques Dans les Écoulements Détendus à Haute Enthalpie: Application à la Soufflerie à Arc F4," Ph.D. Thesis (in French), Université de Provence, Marseille, France, Dec. 1999.

[13] Park, C., "Review of Chemical-Kinetic Problems of Future NASA Missions, 1: Earth Entries," *Journal of Thermophysics and Heat Transfer*, Vol. 7, No. 3, 1993, pp. 385–398.

[14] Colonna, G., and Capitelli, M., "Self-Consistent Model of Chemical, Vibrational, Electron Kinetics in Nozzle Expansion," *Journal of Thermophysics and Heat Transfer*, Vol. 15, No. 3, 2001, pp. 308–316.

[15] Colonna, G., and Capitelli, M., "The Influence of Atomic and Molecular Metastable States in High-Enthalpy Nozzle Expansion Nitrogen Flows," *Journal of Physics D: Applied Physics*, Vol. 34, No. 12, 2001, pp. 1812–1818.

[16] Colonna, G., and Capitelli, M., "The Effects of Electric and Magnetic Fields on High Enthalpy Plasma Flows," AIAA Paper 2003-4036, June 2003.

[17] Colonna, G., and Capitelli, M., "Plasma Expansion in Presence of Electric and Magnetic Fields," *Rarefied Gas Dynamics*, edited by M. Capitelli, Vol. 762, AIP Conference Proceedings, Melville, New York, 2004, pp. 1295–1300.

[18] Lino da Silva, M., "Simulation des Propriétés Radiatives du Plasma Entourant un Véhicule Traversant une Atmosphère Planétaire à Vitesse Hypersonique—Application à la Planète Mars," Ph.D. Thesis (in French), Université d'Orléans, Orléans, France, Dec. 2004.

[19] Parker, J. G., "Rotational and Vibrational Relaxation in Diatomic Gases," *Physics of Fluids*, Vol. 2, No. 4, 1959, pp. 449–462.

[20] Millikan, R. C., and White, D. R., "Systematics of Vibrational

Relaxation," *Journal of Chemical Physics*, Vol. 39, No. 12, 1963, pp. 3209–3213.

[21] Losev, S. A., Kozlov, P. V., Kuznetsova, L. A., Makarov, V. N., Romanenko, Yu, V., Surzhikov, S. T., and Zalogin, G. N., "Radiation of Mixture $CO_2 - N_2 -$ Ar in Shock Waves: Experiment and Modelling," *Proceedings of 3rd European Symposium on Aerothermodynamics for Space Vehicles*, edited by R. A. Harris, ESA Publications Division, ESA/ESTEC, Noordwijk, The Netherlands, 1998 pp. 437–444.

[22] Shatalov, O. P., and Losev, S. A., "Modeling of Diatomic Molecules Dissociation Under Quasistationary Conditions," AIAA Paper 97-2579, June 1997.

[23] Wilke, C. R., "A Viscosity Equation for Gas Mixtures," *Journal of Chemical Physics*, Vol. 18, No. 4, 1950, pp. 517–519.

[24] Chapman, S., and Cowling, T. G., *Mathematical Theory of Non-Uniform Gases*, Cambridge Univ. Press, Cambridge, England, U.K., 1952.

[25] Blottner, F. G., Johnson, M., and Ellis, M., "Chemically Reacting Viscous Flow Program for Multicomponent Gas Mixture," Tech. Report Sc-RR-70-754, Sandia Laboratories, 1970.

[26] Alexandrova, T., "Vibrational and Chemical Nonequilibrium Kinetics in Diatomic Expanding Gas," Ph.D. Thesis, IUSTI, Université de Provence, Marseille, France, Jan. 2002.

[27] D'Ambrosio, D., Colonna, G., and Capitelli, M., "Numerical Prediction of Non-Equilibrium Flows in Hypersonic Nozzles: State-to-State Kinetics Versus Macroscopic Models," AIAA Paper 2003-3549, June 2003.

[28] Bird, G. A., *Molecular Gas Dynamics and the Direct Simulation of Gas Flows*, Oxford Engineering Science Series, Vol. 42, Oxford Science Publications, Oxford, 1994.

[29] Park, C., *Nonequilibrium Hypersonic Aerothermodynamics*, John Wiley & Sons, New York, 1989.

[30] Mazouffre, S., Caubet–Hilloutou, V., and Lengrand, J. C., "Examination of the Shock Wave Regular Reflexion Phenomenon in a Rarefied Supersonic Plasma Flow," *Physics of Plasmas*, Vol. 12, No. 1, 2005, pp. 012323–1–9.

[31] Asselin, P., Cayet, S., Lasgorceix, P., Lago, V., and Dudeck, M., "Mass Spectrometric and Electrostatic Probes Measurements of $N_2 - O_2$ Plasma Flow," *Journal of Thermophysics and Heat Transfer*, Vol. 9, No. 3, 1995, pp. 416–421.

[32] Boubert, P., "Méthodes Spectroscopiques Appliquées aux Plasmas et aux Milieux à Haute Enthalpie," Ph.D. Thesis (in French), Université de Rouen, Rouen, France, Sept. 1999.

[33] Brinkman, E. A., Raiche, G. A., Brown, M. S., and Jeffries, J. B., "Optical Diagnostics for Temperature Measurement in a DC Arcjet Reactor Used for Diamond Deposition," *Applied Physics B: Lasers and Optics*, Vol. 64, No. 6, 1997, pp. 689–697.

[34] Wakisaka, A., Gaumet, J. J., Shimizu, Y., Tamori, Y., Sato, H., and Tokumaru, K., "Growth of Carbon Clusters. The Simplest Process, $2C_1 \rightarrow C_2$, Observed via Spectrometry and Chemical Reaction," *Journal of the Chemical Society, Faraday Transactions*, Vol. 89, No. 7, 1993, pp. 1001–1005.

[35] Lino da Silva, M., and Dudeck, M., "A Line-by-Line Spectroscopic Code for the Simulation of Plasma Radiation During Planetary Entries: The SESAM Code," AIAA Paper 2004-2157, Jul. 2004.

[36] Alexandrova, T., Izrar, B., Lino da Silva, M., and Dudeck, M., "Modelling of Arc-Jet Plasma Flow in Transitional Regime by Navier-Stokes and State-to-State Coupling," *Rarefied Gas Dynamics*, edited by M. Capitelli, Vol. 762, AIP Conference Proceedings, Melville, New York, 2004, pp. 1125–1130.

[37] Kustova, E. V., and Nagnibeda, E. A., "State-to-State Theory of Vibrational Kinetics and Dissociation in Three Atomic Gases," *Rarefied Gas Dynamics*, edited by T. J. Barthel and M. A. Gallis, Vol. 585, AIP Conference Proceedings, Melville, New York, 2001, pp. 620–627.